ACS Sustainable Chemistry & Engineering

Research Article

Cite This: ACS Sustainable Chem. Eng. 2019, 7, 4147−4157

pubs.acs.org/journal/ascecg

Biodegradable UV-Blocking Films through Core−Shell Lignin−Melanin Nanoparticles in Poly(butylene adipate-*co*-terephthalate)

Qianqiu Xing,[†,‡] Pietro Buono,[‡] David Ruch,[‡] Philippe Dubois,*[,‡,§] Linbo Wu,*[,∥] and Wen-Jun Wang*[,†]

[†]State Key Lab of Chemical Engineering, College of Chemical and Biological Engineering, Zhejiang University, 38 Zheda Road, Hangzhou 310027, China

[‡]Department of Materials Research and Technology (MRT), Luxembourg Institute of Science and Technology (LIST), 5 avenue des Hauts-Fourneaux, L-4362 Esch-sur-Alzette, Luxembourg

[§]Center of Innovation and Research in Materials & Polymers (CIRMAP), University of Mons (UMONS), 23 Place du Parc, B-7000 Mons, Belgium

[∥]Key Laboratory of Biomass Chemical Engineering of Ministry of Education, College of Chemical and Biological Engineering, Zhejiang University, 38 Zheda Road, Hangzhou 310027, China

Supporting Information

ABSTRACT: Biodegradable and renewable UV-shielding films are highly demanded to meet the increasing sustainable requirement for the environment. Lignin as a natural broad UV blocker has gained considerable attention; however, the poor dispersibility within synthetic polymers limited its applications. Thus, a bioinspired melanin-like polydopamine thin layer was incorporated for the first time with lignin nanoparticle (LNP) in this effort, forming a UV-blocking core−shell lignin−melanin nanoparticle (LMNP) with higher compatibility and durability. Subsequently, LNP, LMNP, melanin nanoparticles (MNP), and a mix of LNP and MNP (MixNP) were compounded with poly(butylene adipate-*co*-terephthalate) (PBAT), to enhance the UV-barrier capability and photostability of PBAT films. The incorporated LMNPs were well distributed into PBAT, leading to improved tensile properties and thermal stability of the resulting films. All these films possessed remarkable UV-blocking capacity at NP concentration ranging from 0.5 to 5 wt %, blocking almost all of UV-A and more than 80% of UV-B light, while an appreciable optical transmittance could also be achieved. The PBAT−LMNP films displayed a high UV-shielding stability and the best retention in mechanical properties after UV exposure for 40 h. This work provides a very promising approach for fabricating biodegradable PBAT-based UV-blocking films for potential applications in agricultural or food packaging materials where the UV resistance is highly required.

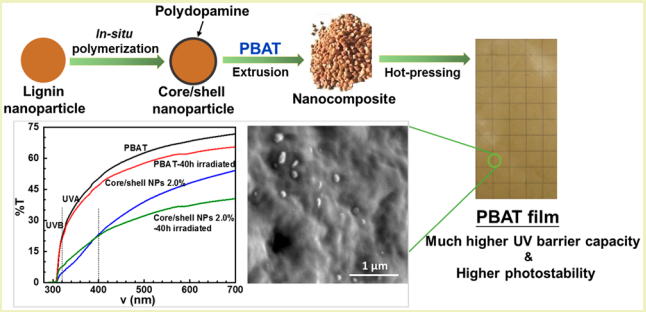

KEYWORDS: *Melanin, Lignin, Core−shell nanoparticles, Poly(butylene adipate-co-terephthalate), Biodegradable UV-blocking film, Photostability*

INTRODUCTION

UV radiation is responsible for the photodegradation of polymeric materials, leading to yellowing and deterioration of mechanical properties.[1,2] Therefore, organic UV absorbers or inorganic UV blockers have been extensively used for protecting polymeric materials from UV radiation. Traditional organic UV absorbers, such as octinoxiate, oxybenzone, and avobenzone, offer good UV resistances. However, they could form aggregate and migrate in polymer matrixes, and some of them even have negative effects on human health or the environment.[3,4] Metal oxide nanoparticles, such as TiO_2, CeO_2, SiO_2, and ZnO, are unable to absorb lights at lower energies than their inherent band gaps, resulting in incomplete UV blocking,[5] and often have photocatalytic effects on polymer matrixes.[6]

Natural compounds with radiation protective properties have gained considerable attention.[7,8] Among them is lignin that can be extracted from agricultural waste and is rich in aromatic rings, which is the second most abundant renewable biomass on the Earth.[9,10] The phenolic units, ketones, and chromophores in lignin structure make it a natural broad UV blocker to screen almost the whole spectrum of UV light.[11,12] Lignin can also act as an antimicrobial and antifungal agent and also an antioxidant.[13,14] Despite its numerous advantages, the untreated lignin has poor dispersibility within synthetic polymers due to the $\pi-\pi$ stacking aromatic rings and hydrogen

Received: November 6, 2018
Revised: January 8, 2019
Published: January 30, 2019

DOI: 10.1021/acssuschemeng.8b05755
ACS Sustainable Chem. Eng. 2019, 7, 4147−4157

bonds between lignin chains,[15−17] exhibiting detrimental impact on the properties of the resulting composites. In addition, the large particle size of commercial lignin limits its more extensive applications in composite materials. Therefore, acidolysis,[18] nanoprecipitation,[19] sonication,[20] and hydroxymethylation approaches[21] have been used to synthesize lignin nanoparticles (LNP) for making polymer−lignin nanocomposites. Possessing higher radical scavenging activity,[22] the lignin NPs (LNP) can significantly improve the thermo-mechanical properties of nanocomposites based on polymers such as poly(vinyl alcohol),[23] phenolic foams,[24] polylactic acid,[25] and wheat gluten.[26] However, it was reported that as-prepared LNP tended to degrade under UV irradiation, and their degradation products had negative effect on the material performances.[25,27] Therefore, stable LNP under irradiation are crucial for their usage as UV blocker.

Melanin is a well-known biomacromolecule present in almost all living organisms. Aside from its biological functions, it displays many attractive features, such as photoprotection, thermoregulation, metal-ion chelation, and free-radical scavenging.[28,29] The incorporation of sepia eumelanin in poly(vinyl alcohol) films could remarkably enhance the UV-shielding properties and photostability.[30] The functional groups, such as −OH, −NH, and −COOH, in melanin allow the formation of strong hydrogen bonding with polymer chains containing polar groups, achieving dramatic enhancement in mechanical properties for the resulting nanocomposites.[31] Artificial melanin-like NPs are usually prepared through auto-oxidation of dopamine in alkaline aqueous solution, resulting in cross-linked polymers having similar chemical and physical properties to natural melanin.[32] Moreover, polydopamine (PDA) can deposit spontaneously on the surface of a wide range of inorganic and organic materials, forming durable thin PDA films.[33] This provides a facile method for surface treatments and gives possibility to produce materials with complex structures, like capsule and core−shell,[34,35] which is expected to be applicable for making core−shell photostable LNP. The synergetic effects of lignin and melanin on enhancing the UV-blocking property and stability are discussed, allowing for a reduced usage of NP.

As a promising biodegradable copolyester, poly(butylene adipate-*co*-terephthalate) (PBAT) possessed good mechanical properties which are comparable to those of polyethylene.[36] A lot of works have been conducted on PBAT in the last decades for its applications in agricultural, food packaging, and biomedical areas.[37,38] However, its poor photostability leads to the severe deterioration of its mechanical performance during applications, which remains as the major limitation for PBAT usage, especially as mulching films.[39,40] In our previous work,[41] modified SLs with 10-undecenoic and oleic acids were used for improving photostability of PBAT. The resulting films possessed excellent UV protection on the whole range of 280−400 nm. But high loadings of modified SL (>10 wt %) were required due to SL dispersed in PBAT matrix having large particle sizes (∼10 μm), leading to poor transparency of the films.

Herein, a lignin nanoparticle is introduced for enhancing the UV barrier property of PBAT while reducing the SL loading. The LNP were coated with a layer of rigid UV-resistance PDA to form core−shell lignin−melanin NPs (LMNP) via in situ polymerization of dopamine on the surface of LNP. The LMNPs were blended with PBAT to prepare films via compression molding. The deposition of the PDA on the LNP surfaces was examined by X-ray photoelectron spectroscopy (XPS), FTIR, and elemental analysis (EA). The SEM measurement was used to investigate the dispersion of the LMNP in the PBAT matrixes. Tensile properties and thermal stabilities of the resulting nanocomposite films were evaluated. UV-blocking capacity and photostability of the PBAT nanocomposite films were also investigated.

EXPERIMENTAL SECTION

Materials. Sulfur-free alkaline soda lignin (SL, Protobind 1000) is supplied by Green Value SA (Switzerland). It is obtained from a mixture of wheat straw (*Triticum sp.*) and Sarkanda grass (*Saccharum officiarum*) by extraction and fractionation following a patented process.[42] The SL has a low molecular weight with low residual ether bonds and high degree of condensation.[43] As reported by Buono et al., the lignin has a number-average molecular weight (M_n) of 838 g·mol^{-1} and initial −OH content of 5.2 mmol·g^{-1} estimated from ^{31}P NMR.[44] The SL was used as received without further purification.

Dopamine hydrochloride was purchased from Sigma-Aldrich, sodium hydroxide (>99%) from Carl Roth, Tris (99.96%) from Euromedex, and acetone (>95%) from Acros Organics. All chemicals were used as received.

Poly(butylene adipate-*co*-terephthalate) (PBAT) pellets (Biocosafe 2003 F) were kindly provided by Xinfu Pharmaceutical Co., Ltd., China. The pellets have a mole ratio of aromatic to adipic of 45:55, M_n of 39 700 g·mol^{-1}, polydispersity index of 2.9, density of 1.26 g·cm^{-3}, and melt index of 3.5 deg·min^{-1} (ISO 1133, 190 °C/2.16 kg). They were dried under vacuum at 50 °C for 24 h prior to use.

Preparation of Nanoparticles. *Lignin Nanoparticles.* The LNP were prepared following the procedure reported by Yearla et al.[19] In brief, SL (10 mg/mL) was dissolved in acetone and water (9:1, v/v) and filtered through a 0.2 μm Millipore membrane to remove undissolved particles. The filtrate was added rapidly (<1 min) to deionized water with a volume proportion of 1:2.66 at a stirring speed of 500 rpm. Parallel experiments with a volume ratio (filtrate/water) of 1/2, 1/3, and 1/4 were also conducted. After continuous stirring for 30 min at 20 °C, acetone was removed under vacuum by rotary evaporation (Buchi Rotavapor R-205, Hampton, U.S.A.). The suspension was then centrifuged (Sigma 3K30, Osterode am Harz, Germany) at 20 °C and 5000 rpm for 15 min to remove the aggregates. The LNP were easily retrieved from the supernatant after centrifugation (40 min, 16500 rpm, 5 °C) and redispersion processes in deionized water. The LNP were further used for the synthesis of lignin−melanin core−shell nanoparticles LMNP and the following preparation of PBAT−LNP composites.

Lignin−Melanin Core−Shell Nanoparticles. After the removal of larger LNP aggregates using low speed centrifugation (5 min, 5000 rpm, 20 °C), a given amount of dopamine hydrochloride was dissolved in the supernatant at a concentration of 1 g·L^{-1}, followed by an adjustment of pH value to 8.0 using Tris buffer (30 mM). The reaction was allowed to proceed for 24 h at 35 °C under constant stirring. The collection and purification of LMNP were conducted under the same conditions used for the preparation of the LNP.

Melanin Nanoparticles (MNP). The MNP were prepared following the protocol of Ju et al.[45] Specifically, dopamine hydrochloride (270 mg) was dissolved in 300 mL of deionized water. Under vigorous stirring, 1.8 mL of 1 N NaOH solution was added at 70 °C. The color of the solution turned into pale yellow when NaOH was added and changed to dark brown afterward. After 2.5 h, low-speed centrifugation at 5000 rpm and 20 °C for 15 min was used to remove large particles. The MNP were then retrieved by centrifugation at 16 500 rpm and 5 °C for 30 min and washed repeatedly with deionized water.

Preparations of Films. The PBAT resin was compounded with 10 wt % LNP, LMNP, a mixture of MNP and LNP at 14.1:85.9 in weight (MixNP), and MNP, respectively, in a twin-screw micro-compounder (Xplore 15 cc, DSM, Geleen, Netherlands) for making masterbatches. Ten grams of masterbatch and PBAT blends at various ratios were prepared batchwise in the microcompounder at 130 °C for

DOI: 10.1021/acssuschemeng.8b05755
ACS Sustainable Chem. Eng. 2019, 7, 4147−4157

Scheme 1. Schematic Illustration of the Procedure for the Preparation of Lignin (LNP) and Lignin−Melanin Core−Shell Nanoparticles (LMNP)

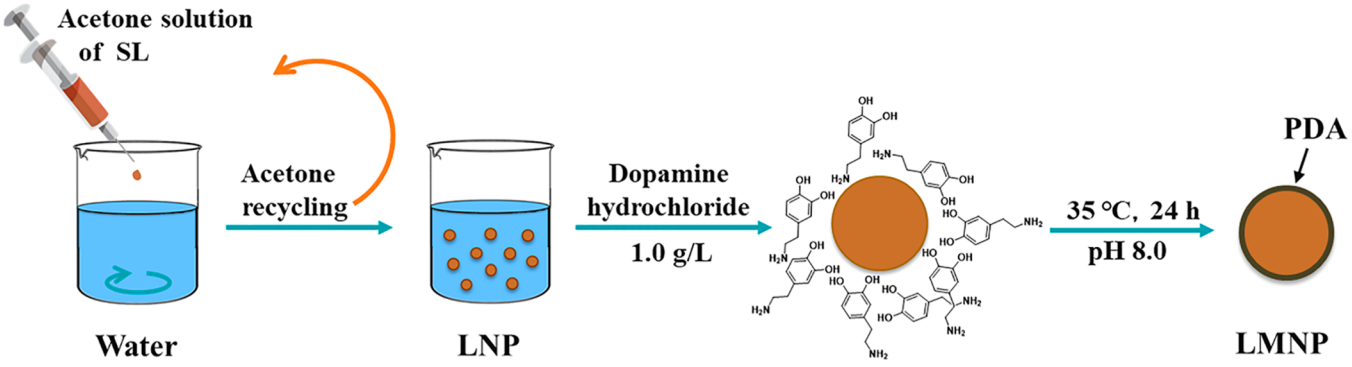

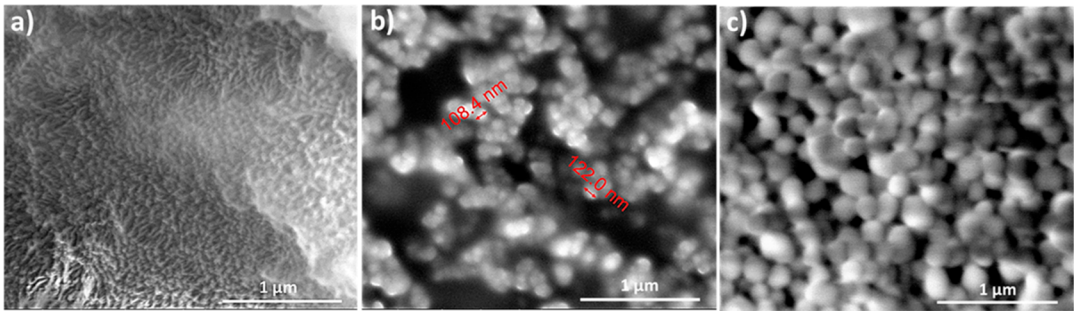

Figure 1. SEM images of nanoparticles retrieved by centrifugation: (a) LNP, (b) LMNP, and (c) MNP.

an extrusion time of 7 min with recirculation under N_2 and screw speed of 100 rpm. The PBAT−NP composites strands with 0.5, 1.0, 2.0, and 5.0 wt % NP loading were extruded and cut into pellets with a diameter of 3−5 mm and length of 3 mm. The pellets were pressed with a Carver 3851-0 hot press machine (Wabash, U.S.A.) at 140 °C and 400 bar for 5 min and cooled down to room temperature under the same pressure to prepare films with thickness of approximately 50 μm. Neat PBAT films were also made as reference.

Irradiation of Films. All films were irradiated for 40 h in a Suntest CPS+ chamber (Atlas, Linsengericht, Germany), using a xenon lamp and solar standard filter (filter according to COLIPA and DIN 67501). The measurement condition was simple daylight 400 $W{\cdot}m^{-2}$ and black panel temperature at 63 °C.

Characterization. *Elemental Analysis, EA.* The elemental compositions of the NPs were determined using a Truspec CHN analyzer (Leco, Saint Joseph, U.S.A.), based on catalytic combustion at 950 °C followed by infrared (C, H) and thermal conductivity (N) detection. The instrument was calibrated using certified BBOT (2,5-bis(5-tertbutylbenzoxazol-2-yl) thiophene).

X-ray Photoelectron Spectroscopy, XPS. The chemical compositions of the NP surfaces were determined using XPS. The measurements were carried out on a VG ESCALAB MARK II spectrometer (VG Instruments Inc., Stanford, U.K.) with a Mg Kα X-ray source (photon energy: 1253.6 eV). The spectra were acquired in a CAE mode (constant analyzer energy) with analyzer pass energies of 50 eV, with a step size of 0.2 e V for the C 1s, N 1s, and O 1s photoelectron lines and 0.5 eV for survey scans in the range of 0−1000 eV.

FTIR and UV−Vis Absorption Spectroscopy. The FTIR-ATR spectra in the wavelength range of 4000−400 cm^{-1} were acquired at a resolution of 4 cm^{-1} using a Bruker Tensor 27 spectrometer (Ettlingen, Germany). The transparencies of the PBAT and PBAT−NP films in the 280−800 nm range were measured with a Lambda 35 UV/vis spectrometer (PerkinElmer, Shelton, U.S.A.).

Dynamic Light Scattering Analysis (DLS). The *z*-average particle sizes and particle size dispersities of the NPs were characterized using a Malvern Zetasizer ZEN 3600 instrument (Malvern Instruments Ltd., Worcestershire, U.K.). The samples were prepared by diluting the reaction solutions of the NPs before centrifugation in deionized water.

Thermogravimetric Analysis (TGA). TGA tests of all the NPs, PBAT−NP composites, and PBAT as-prepared were conducted using a STA 409PC Luxx apparatus of NETZSCH (Selb, Germany). Approximately 30 mg of sample was heated to 800 °C at a rate of 10 $°C{\cdot}min^{-1}$ under nitrogen atmosphere.

Differential Scanning Calorimetry (DSC). The DSC measurements for all the predried PBAT and PBAT−NP composites were carried out on a TA DSC Q200 calorimeter (TA Instruments) under nitrogen atmosphere, with typical heating/cooling/heating cycles from −70 to 180 °C at a heating/cooling rate of 10 $°C{\cdot}min^{-1}$. The glass transition temperature (T_g) and melting temperature (T_m) were obtained on the second heating run, while the melt crystallization enthalpy (ΔH_c) was collected on the cooling run.

Uniaxial Tensile Test. Tensile properties of the films were measured by an Instron 5967 universal testing machine (Norwood, MA, U.S.A.) at room temperature according to ASTM D882. The samples were dried overnight at 40 °C under vacuum and preconditioned for the following 2 days in the measurement environmental conditions. For each sample, five dumbbell shaped specimens with the width of 12.5 mm and length of 75 mm were tested. The drawing speed was set at 50 $mm{\cdot}min^{-1}$.

Scanning Electron Microscopy (SEM). The SEM images of all NPs, cross sections of all PBAT−NP composites, and PBAT as-prepared were obtained on a Quanta FEG 200 environmental SEM (FEI, Eindhoven, Netherlands). The extruded strands were fractured in liquid nitrogen, and the fractured surfaces were observed. The images were obtained under 150 Pa pressure, acceleration voltage of 6 kV, and electron beam spot size of 9.7−10.0.

RESULTS AND DISCUSSION

Preparation and Characterization of NPs. A nanoprecipitation method was employed to fabricate LNP. The nanoprecipitation is known as a green, facile, low energy input,

DOI: 10.1021/acssuschemeng.8b05755
ACS Sustainable Chem. Eng. 2019, 7, 4147−4157

and relatively quick process to prepare polymeric nanoparticles.[46] In brief, a polymer is dissolved in a water miscible organic phase and subsequently mixed with an aqueous solvent, triggering the precipitation of the polymer to form nanoparticles with controlled sizes and dispersity.[47,48] In our work, the dispersions obtained from the nanoprecipitation process either underwent centrifugation to collect the LNP or served as seed and reaction media for the preparation of LMNP (Scheme 1). During the polymerization of dopamine for the preparation of LMNP, the color of the dispersions changed from beige to dark brown. To date, the mechanism for dopamine polymerization process is still not fully understood. Herlinger et al. proposed a mechanism in which, in the presence of O_2 and basic condition, the hydroquinone group of dopamine deprotonates and oxidizes to be dopamine quinone, which in turn becomes leuco-dopamine chrome via intramolecular cyclization. Leuco-dopamine chrome then forms 5,6-dihydroxyindole by oxidation and rearrangement to yield the insoluble cross-linked polymeric materials known as "melanin".[49] It is expected that the catechol groups in the PDA shell can covalently interact with lignin given the abundance of hydroxyl groups on its surface.[33,50,51]

The surface topography images of the LNP, MNP, and core−shell LMNP were observed by SEM as shown in Figure 1. Although all the NPs could be well dispersed in water, Figure 1a shows that the LNP appeared to form a bulk of aggregated particles without clear interfacial boundaries after centrifugation. By deposition of PDA on the surface of LNP, the spherical shape of LMNP could be clearly observed (ca. 110 nm, Figure 1 b) and is analogous to the MNP (ca. 183 nm, Figure 1 c). The presence of closely covered PDA layers endowed higher rigidity to LMNP, resulting in a surface topography change for the LNP.[45] The DLS analysis was also carried out for the NPs to measure their particle sizes in water. As depicted in Figure 2, the DLS curves show that the average

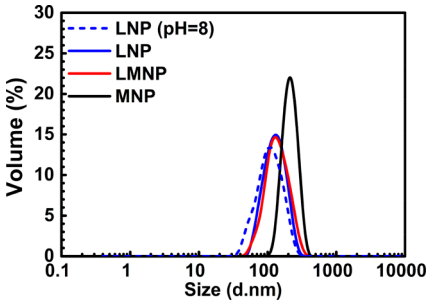

Figure 2. Particle size distribution of nanoparticles determined by DLS.

sizes of LNP, LMNP, and MNP are ca. 124, 125, and 200 nm, respectively. For the LMNP and MNP, the weight-average sizes determined by DLS are slightly larger than those obtained from the SEM, which are number-average based. The addition of the Tris buffer in the LNP dispersion, which triggered the subsequent PDA deposition, resulted in decrease of the LNP sizes from approximately 124 to 118 nm (Figure 2). This might due to partial dissolution of the LNP with increasing pH since the SL is more soluble under basic conditions than under acidic or neutral ones.

The influence of the experimental conditions on the LNP sizes was also investigated by the DLS. Figure S1 shows that the LNP sizes decreased from 150 to 75 nm when the ratios between the filtrate and water were changed from 1:2 to 1:4.

The surface chemical compositions for different NPs were determined by XPS. Efficient deposition of PDA on the LNP surfaces was verified by the appearance of N 1s signal in the spectrum of the LMNP, which was absent in the LNP prior to PDA coating (Figure 3). Two peaks were evidenced via the

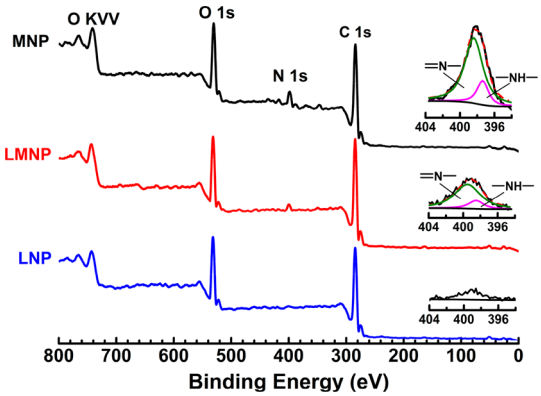

Figure 3. X-ray photoelectron spectroscopy wide scans for the LNP, LMNP, and MNP. The inset highlights the N 1s core-level spectra.

curve deconvolution of N 1s core-level spectra of the MNP and LMNP, which could be attributed to N_{imine} (═N—, 398.5 eV) and N_{amine} (—NH—, 399.5 eV), respectively. The percentages of N_{imine} and N_{amine} in the LMNP were 81 and 19%, respectively, which were the same as those in the MNP (83 and 17%), suggesting the formation of a PDA layer on the LNP. The nitrogen-to-carbon signal ratio (N/C) was also estimated to be 0.133 for the MNP, which is close to the theoretical value of 0.125 for dopamine.[33] However, the N/C ratio for the LMNP was 0.081, suggesting an incomplete coverage of PDA on the LNP surfaces, likely due to the formation of thin and rough layers in several nanometers.[52]

The FTIR spectra of the LNP, LMNP, and MNP were collected as shown in Figure 4. The LNP show a broad peak

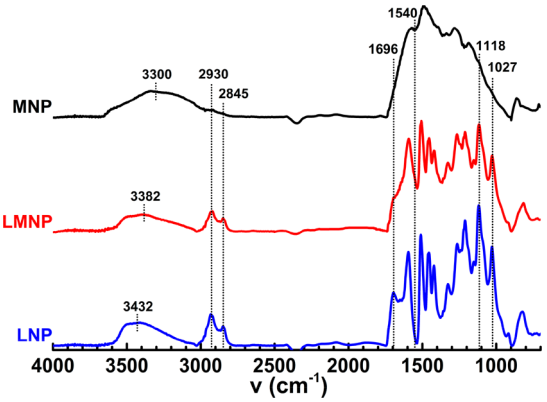

Figure 4. FTIR spectra for the LNP, LMNP, and MNP.

from 3594 to 3026 cm^{-1}, belonging to the phenolic and aliphatic O−H stretching. The signals located at 2930 and 2849 cm^{-1} mainly arise from aliphatic C−H stretching. Another distinctive resonance at 1696 cm^{-1} originates from the conjugated carbonyl stretching. The peaks at 1118 and 1027 cm^{-1} are indicative of the in-plane deformation of aromatic C−H from syringyl (S) and guaiacyl (G) structures,

DOI: 10.1021/acssuschemeng.8b05755
ACS Sustainable Chem. Eng. 2019, 7, 4147−4157

respectively, together with their out of plane bending appearing at 815 cm^{-1}.[53] The MNP have no overlapping peaks to the lignin footprints, with the exception of a broad signal present above 3000 cm^{-1}. The predominant N−H stretching can be observed at 3330 cm^{-1}. The peculiar C═N stretching at 1540 cm^{-1} indicates the presence of aromatic amine species.[54] The LMNP show a very similar FTIR spectrum to the LNP, with decrease of relative intensities for the aliphatic C−H stretching (at 2925 and 2847 cm^{-1}), conjugated C═O stretching (at 1696 cm^{-1}), and C−H deformation of G and S (at 1118 and 1027 cm^{-1}). The broad band peak above 3000 cm^{-1} shifts from approximately 3450 to 3380 cm^{-1} with the formation of PDA, confirming the presence of N−H stretching. The C═N stretching appears at 1540 cm^{-1}.

To determine the weight ratio of lignin and PDA in the LMNP, the EA measurements were conducted for the MNP, LMNP, and LNP. The weight percentages of N, C, and H for all samples are summarized in Table 1. The MNP had the highest N content (~8.52 wt %) among the three samples, while only a trace amount of N (~0.62 wt %) was detected in LNP. The LMNP had an N content of 1.73 wt %. From the N values of the three samples, the weight percentage of PDA (χ_{PDA}) in the LMNP can be estimated using eq 1.

Table 1. Elemental Compositions in the LNP, LMNP, and MNP Obtained with Combustion Elemental Analysis

	mean ± SD (wt %)		
sample	N	C	H
LNP	0.6 ± 0.0	67.4 ± 0.1	5.7 ± 0.0
LMNP	1.7 ± 0.0	64.3 ± 1.5	5.8 ± 0.2
MNP	8.5 ± 0.0	56.1 ± 0.5	3.5 ± 0.1

$$\chi_{PDA}(\%) = \frac{[N]_{LMNP} - [N]_{LNP}}{[N]_{MNP} - [N]_{LNP}} \times 100 \quad (1)$$

where $[N]_{LMNP}$, $[N]_{LNP}$, and $[N]_{MNP}$ refer to the contents of N in the corresponding NPs, respectively. Using eq 1, the χ_{PDA} in the LMNP was obtained as 14.1 wt %. The contents of C and H in the LMNP can thus be estimated as 65.8 and 5.4 wt %, respectively, which are consistent with the measured values of 64.3 and 5.8 wt %.

Thermal degradation behaviors of the LNP, LMNP, and MNP were also investigated under nitrogen atmosphere (Figure 5). All the samples displayed multistep weight loss. The LNP had small mass loss between 90 and 120 °C, corresponding to the removal of residual water.[44] The value of $T_{d,5}$ (calculated at mass loss of 5%) was 223.5 °C, which appeared at a slightly lower temperature compared to neat lignin of 235.8 °C. The char yield at 800 °C reduced markedly from 44.0% of SL to 35.4%,[41] which could be attributed to the removal of undissolved fraction during the preparation of the LNP. The MNP also displayed a weight loss at less than 100 °C owing to high hygroscopicity of melanin.[55] The PDA layer on the surface of LNP dramatically increased its thermal stability despite the PDA constituting only 14 wt % of LMNP. The mass loss between 230 and 480 °C was considerably reduced, and the char yield was very close to that of the MNP value of 50.0 wt %.

PBAT−NP Nanocomposites. The LNP, LMNP, a mixture of MNP and LNP at 14.1:85.9 in weight (MixNP), and MNP were melt-blended with PBAT at 0.5, 1.0, 2.0, and 5.0 wt % loading. The resulting composites were analyzed to investigate the influence of the NPs on the thermal, physical, and morphological properties of PBAT.

SEM micrographs of the cryo-fractured surfaces of the PBAT nanocomposites are presented in Figure 6. All the NPs, independent of their nature, could be easily dispersed in the PBAT matrix at 5 wt % loadings. The LNP, although agglomerated after the centrifugation (Figure 1 a), showed a good dispersibility in the PBAT matrixes, suggesting a better compatibility with polyester materials than the SL.[53] The LMNP (Figure 6b) were stable under vigorous shearing during the extrusion, and few PDA shells were broken during the process, suggesting a strong adhesion between PDA and SL through the covalent interactions. The MixNP with PBAT (Figure 6c) showed no aggregation between lignin and melanin NPs. However, for nanocomposites with 5.0 wt % MNP (Figure 6d), some NP agglomerations are found across the fractured surfaces, suggesting the presence of SL promotes the dispersibility of PDA material in PBAT.

The thermal stabilities of the PBAT nanocomposites from 0.5 to 5 wt % NP loadings were evaluated by TGA, and the results are shown in Figures 7 and S2. The $T_{d,5}$ and residual mass at 750 °C are summarized in Table 2. It can be seen that PBAT underwent a one-step degradation process with an initial decomposition temperature $T_{d,5}$ of 369 °C and a major weight loss occurring around 400 °C as evidenced by the DTG curves (inset plots of Figure 7). Except for the sample containing 0.5 wt % of MNP, the thermal stability of the whole set of nanocomposites showed a slight increase compared to the neat PBAT, which is attributed to the contribution from

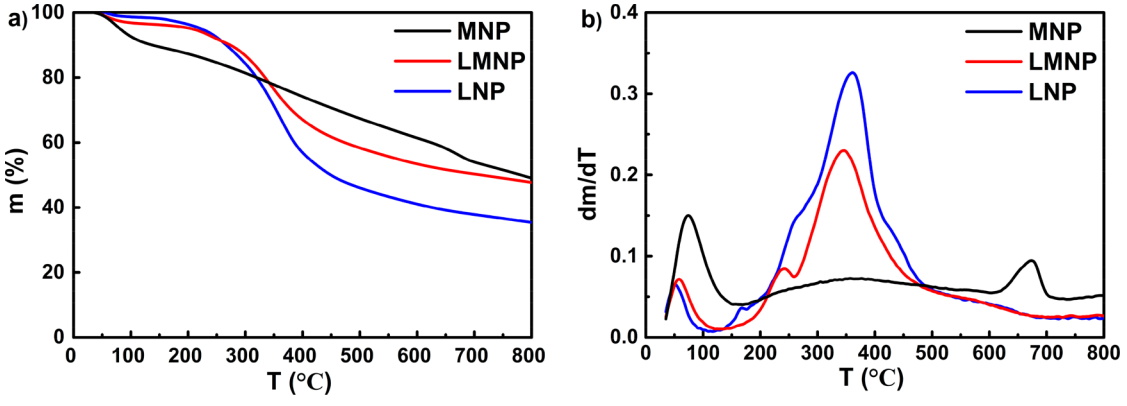

Figure 5. TGA (a) and DTA (b) thermograms of the LNP, LMNP, and MNP.

DOI: 10.1021/acssuschemeng.8b05755
ACS Sustainable Chem. Eng. 2019, 7, 4147−4157

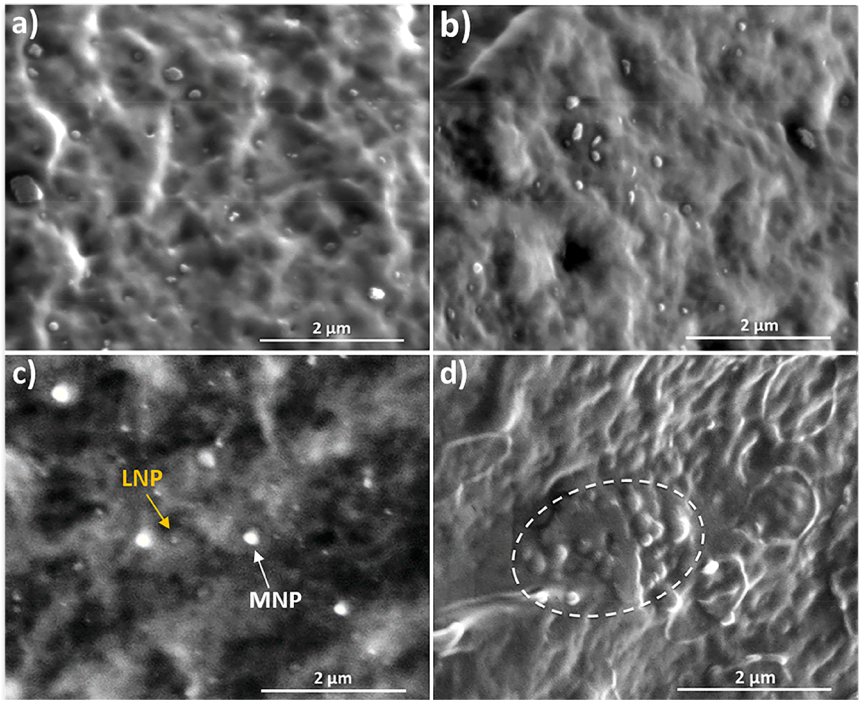

Figure 6. SEM images of cryo-fractures of PBAT−NP nanocomposites (a) LNP, (b) LMNP, (c) MixNP, and (d) MNP. All samples contain 5.0 wt % of NPs.

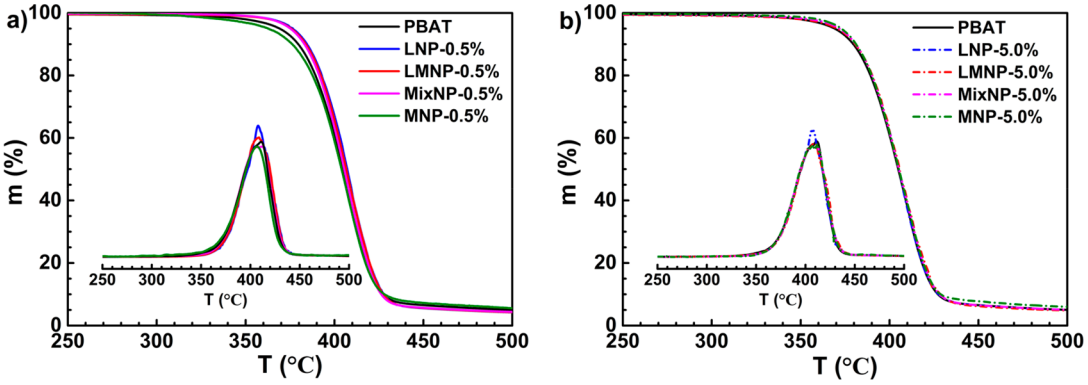

Figure 7. TGA and DTG curves in nitrogen for neat PBAT and PBAT−LNP, PBAT−LMNP, and PBAT−MixNP nanocomposites containing (a) 0.5 and (b) 5.0 wt % of NPs.

radical scavenging effects of SL and PDA. As shown in Table 2, the $T_{d,5}$ shifts from 369 °C of PBAT to 371−377 °C of PBAT nanocomposites.[32,56] This enhancement of thermal stability was more obvious at low NP contents and turned to be reduced with the increase of NP loading. For instance, samples containing 5 wt % of NPs had the $T_{d,5}$ very close to neat PBAT, indicating the radical scavenging function of the NP was compromised by their intrinsic thermal degradation.

The DSC analyses were also carried out to investigate the crystallization temperature T_c, glass transition temperature T_g, melting temperature T_m, and enthalpy (ΔH_m) of PBAT and its nanocomposites. The thermograms of cooling and the second heating run of nanocomposites at 0.5 and 5.0 wt % NP loading are shown in Figure 8. The thermograms of nanocomposites at 1.0 and 2.0 wt % NP are also shown in Figure S3. The calorimetric parameters are summarized in Table 2.With the incorporation of NPs in PBAT matrixes, both T_m and ΔH_m changed slightly. Regardless of the nature and composition of the NPs, the T_c of the nanocomposites shifted gradually to lower temperatures with higher NP loading, from 80.9 down to 73.8 °C. The change in crystallinity was relatively minor, similar to other PBAT nanocomposite systems previously reported.[57−59] Except for the MNP samples, the increase of the T_g values upon inclusion of nanofillers was also observed, particularly for composites with MixNP, which is attributed to the interaction between NPs and PBAT to constrain the polymer chain mobility.

Properties of PBAT Nanocomposite Films. A potential application for PBAT nanocomposites is to be used as biodegradable UV blocking films for light-sensitive product packaging. To investigate the UV-blocking properties of the nanocomposites, thin films (approximately 50 μm thickness) were prepared by compression molding and analyzed using UV−vis spectroscopy to examine the UV blocking capacity. As shown in Figure 9, PBAT had poor UV barrier properties toward the UVA range (320−400 nm, but absorbed 92% of UVB light (280−320 nm) and all the range below due to its benzene rings and carbonyl groups.[60] The PBAT nano-

DOI: 10.1021/acssuschemeng.8b05755
ACS Sustainable Chem. Eng. 2019, 7, 4147−4157

Table 2. TGA and DSC Results of PBAT As-Prepared and Its Nanocomposites

	TGA		DSC				
sample	$T_{d,5}$ (°C)	Char (%)	T_c (°C)	ΔH_c (J/g)	T_g (°C)	T_m (°C)	ΔH_m (J/g)
PBAT	369.2	4.0	79.8	13.1	−35.3	118.7	8.5
LNP-0.5%	376.7	3.4	78.1	13.7	−34.2	119.9	7.9
LNP-1.0%	376.5	3.3	78.3	13.5	−32.7	120.2	8.6
LNP-2.0%	376.5	3.4	77.6	13.7	−33.2	119.9	8.5
LNP-5.0%	371.5	4.0	73.8	12.5	−32.5	117.8	9.1
LMNP-0.5%	375.8	3.5	79.4	13.5	−33.3	120.0	8.1
LMNP-1.0%	375.3	3.4	78.2	13.4	−35.0	118.8	8.5
LMNP-2.0%	374.7	3.5	76.7	13.1	−34.3	119.3	8.3
LMNP-5.0%	370.6	3.8	74.6	12.2	−34.2	117.4	8.8
MixNP-0.5%	375.2	3.7	79.6	13.9	−32.9	119.7	8.8
MixNP-1.0%	374.4	3.5	79.2	14.8	−32.2	118.8	8.6
MixNP-2.0%	373.4	3.7	78.2	13.2	−32.6	118.5	8.9
MixNP-5.0%	371.8	4.1	75.7	12.4	−31.7	118.0	8.3
MNP-0.5%	362.5	4.1	80.8	10.9	−35.6	119.3	6.7
MNP-1.0%	371.2	4.2	80.2	11.6	−35.4	118.5	7.4
MNP-2.0%	372.7	4.1	79.7	11.1	−35.5	118.4	7.2
MNP-5.0%	372.8	4.2	78.8	10.9	−34.8	118.8	7.4

composites exhibited better UV barrier properties than PBAT (Figure 9a,c,e,g), and their UV absorptions were reinforced with increasing the NP loading, similar to what was previously reported.[61−64] For samples containing LNP, LMNP, and MixNP, more than 98% of UVB and approximately 80% of UVA light was blocked with 1.0 wt % NP loading. When the NP content was increased to 5 wt %, the absorptions of UVA reached 93−98%. The transparency of the films was also examined. The optical transmittance of neat PBAT was 66% at 550 nm as shown in Figures 9 and S4 and then declined upon the blending of NPs. The LNP at 5 wt % loading had a transparency of 49%, while the values were roughly halved for the LMNP and MixNP composites. In the case of PBAT−MNP films, almost all the UVB lights were blocked. When MNP loadings were more than 1.0 wt %, the absorption of UVA light also reached to nearly 99%. However, the transparency deceased dramatically to only 6%. The films were completely dark.

The nanocomposite films were irradiated for 40 h under UV using a xenon lamp, and their UV−vis light transmittances were analyzed to evaluate the UV blocking properties (Figure 9b,d,f). Due to the extra crystallization induced by photodegradation,[65] the transmittance of the PBAT film within the UV−vis region decreased slightly during UV exposure. The LNP composite films at 1.0−5.0 wt % NP loadings exhibited a gradual reduction in their UV blocking capabilities, from 80−93% down to 58−81%, in UV-A range after the irradiation, suggesting that lignin photodegraded under UV lights.[25,66] The LMNP and MixNP composites exhibited higher retention of UV absorbance than PBAT−LNP after 40 h of irradiation and absorbed 92−94% UV-A light at 5 wt % NP loadings. At lower NP contents, the PBAT−LMNP still exhibited higher UV absorptions than their PBAT−MixNP counterparts. For samples with MNP, good UV blocking remained after 40 h UV exposure. It is no doubt that PDA plays a crucial role in preventing lignin from photodegradation. The core−shell structure further enhances the lignin photostability.

The evaluation of mechanical properties under UV exposure provides direct evidence for the materials durability. The mechanical properties of the PBAT nanocomposites before and after the 40 h of UV irradiation were investigated by tensile testing at room temperature, as shown in Figure 10. The mechanical property results are summarized in Table S1. The tensile strength (σ), Young's modulus (E), and elongation at break (ε) of neat PBAT films were 22 MPa, 49 MPa, and 522%, respectively. The stress−strain curves in Figure S5 show that all the films performed tensile behaviors of crystallizable ductile polymers, with the yielding and necking followed by the strain hardening.

The PBAT−LNP nanocomposite films showed higher stiffness, tensile strength, and elongation at break than those of neat PBAT. In general, rigid nanofillers in soft matrixes improve the stiffness and tensile strength, while reducing the elongation properties.[67,68] Similar behaviors have been reported previously in PLA composites containing lignin NPs.[69−71]

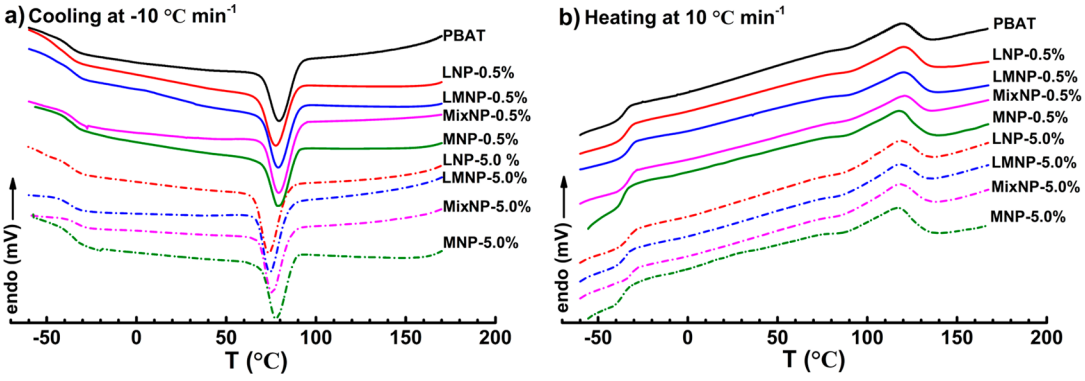

Figure 8. (a) Cooling and (b) second heating DSC curves for PBAT as-prepared and PBAT−LNP, PBAT−LMNP, PBAT−MixNP, and PBAT−MNP nanocomposites with 0.5 and 5.0 wt % NP loadings.

DOI: 10.1021/acssuschemeng.8b05755
ACS Sustainable Chem. Eng. 2019, 7, 4147−4157

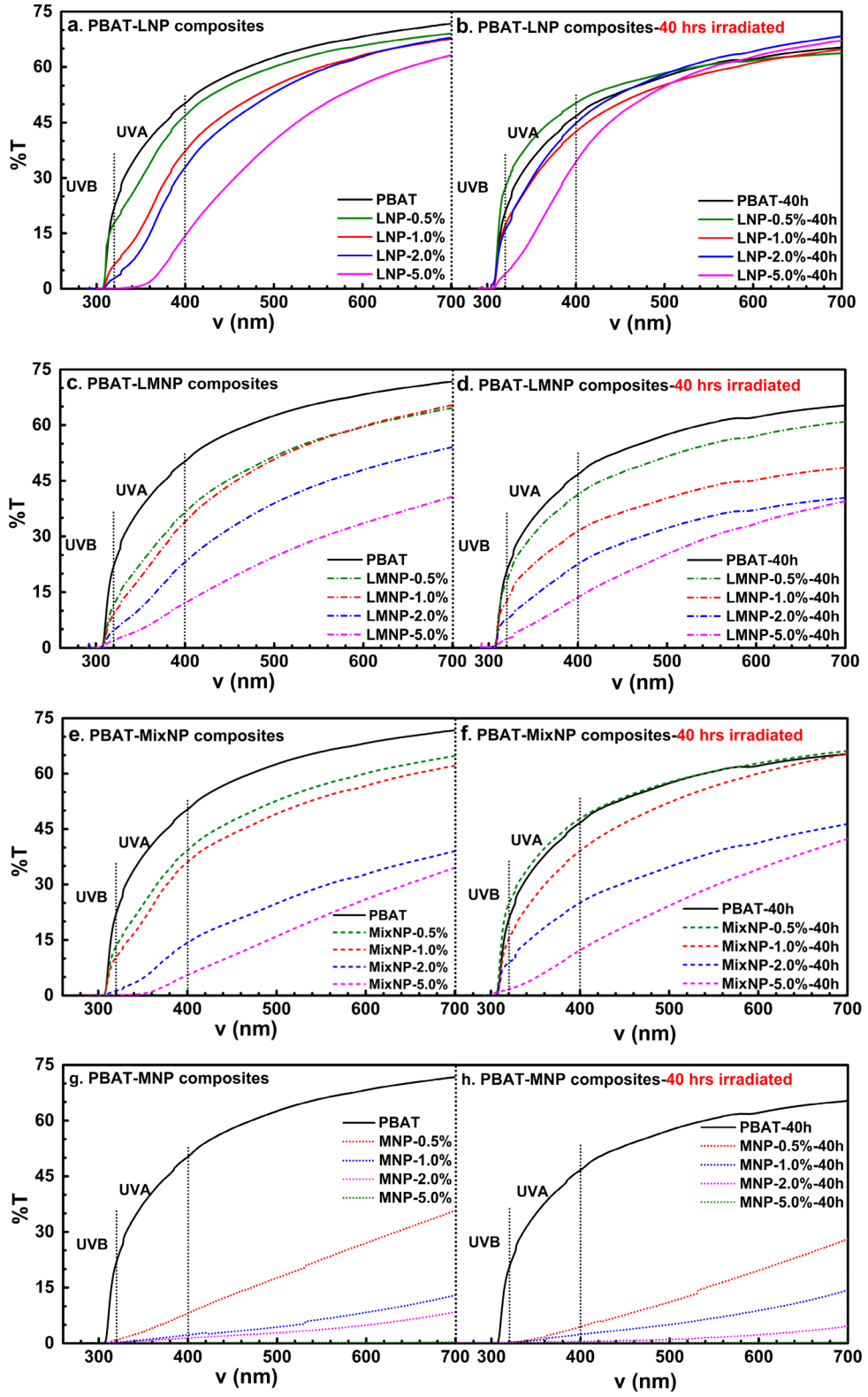

Figure 9. Transmittance of neat PBAT and PBAT nanocomposite films prior to and subsequent to 40 h of UV irradiation: (a and b) PBAT−LNP, (c and d) PBAT−LMNP, (e and f) PBAT−MixNP, and (g and h) PBAT−MNP composites.

The incorporation of LMNP into the PBAT matrix enhanced the mechanical properties of the films even more than that of LNP, due to the higher rigidity of LMNP comparing to LNP as revealed by SEM images in Figure 1a. The ε of PBAT−LMNP blends reached a maximum value 612% at 2.0 wt % LMNP loadings and decreased with increasing loading of NPs, which is in contrast to the increased ε values with high NP loading in the PBAT−LNP. PBAT−MixNP films showed a slightly higher stiffness than neat PBAT, but their tensile strength and elongation at break barely changed. PBAT−MNP composites showed high E values (66−82 MPa) and relatively high σ and ε at lower MNP contents. It

DOI: 10.1021/acssuschemeng.8b05755
ACS Sustainable Chem. Eng. 2019, 7, 4147−4157

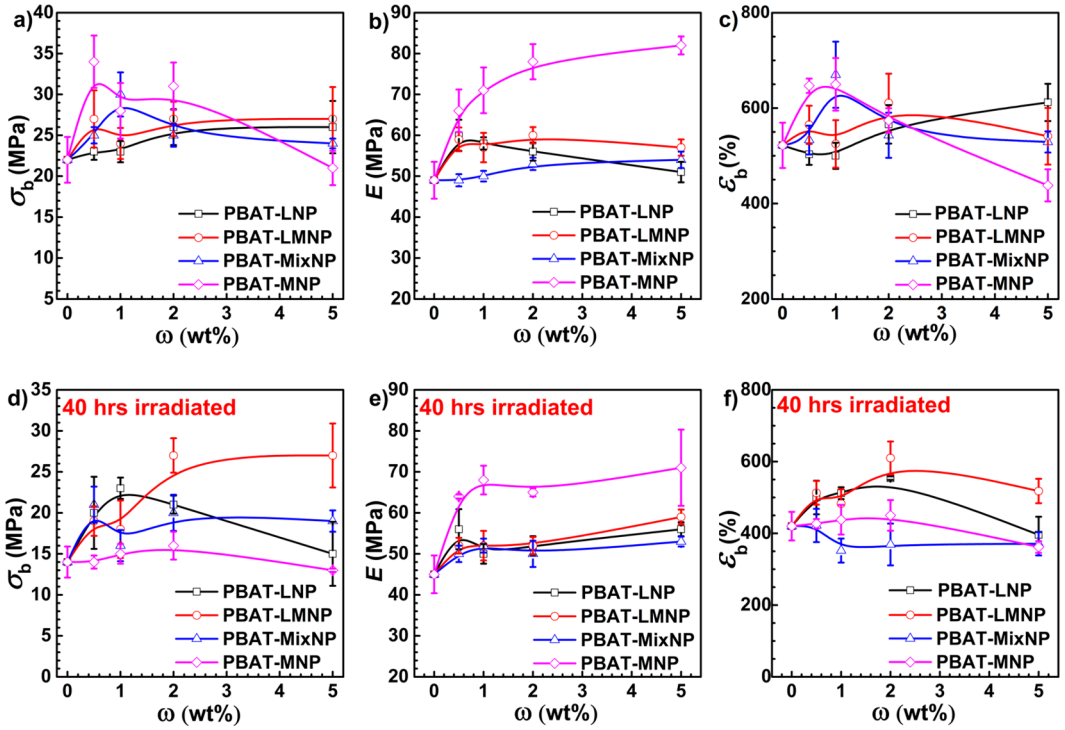

Figure 10. Tensile properties of neat PBAT and PBAT nanocomposite films before and after 40 h of UV irradiation: (a and d) tensile strength, (b and e) Young's modulus, and (c and f) elongation at break.

is no surprise considering that it contains the highest amount of rigid nanoparticles among all samples.

After being exposed under UV light for 40 h, neat PBAT showed deteriorated mechanical properties. The samples containing 0.5−2.0 wt % LNP could retain their tensile strength σ and elongation at break ε after UV exposure. However, for a loading of 5.0 wt % LNP, the mechanical properties could not be retained, and ε decreased from 610% to 400%. Similar results have been observed in PLA, PE, and PP composites with lignin.[25,27,66] PBAT−LMNP nanocomposites showed greater tensile property retention than PBAT−LNP composites with almost unchanged ε subsequent to UV irradiation, especially the composite at 5 wt % NP loadings, despite a very low content (0.28−0.70 wt %) of PDA. When the MixNPs and MNPs were blended into PBAT, regardless of the particles load, all the nanocomposites exhibited similar deteriorated tensile properties after UV irradiation. The findings are quite surprising because the PBAT−MNP nanocomposites contained the highest PDA content among all their counterparts. It demonstrates that a synergistic effect exists between PDA and lignin. The PDA layer inserted between PBAT and lignin stabilizes both polyester and LNP, and the existence of lignin improves the compatibility between PDA and PBAT, thus prolonging PBAT lifetime under UV exposure.

CONCLUSIONS

Core−shell lignin−melanin nanoparticles LMNP were synthesized through spontaneous deposition of polydopamine PDA on the surface of lignin nanoparticles LNP via a nanoprecipitation method. Successful deposition of 14 wt % PDA layer on LNP was confirmed with XPS, FTIR, and EA. The LMNP were proved to possess better thermal stability than LNP. A series of PBAT-based nanocomposites were fabricated by compounding commercial PBAT with LNP, LMNP, MixNP, and MNP through melt extrusion. SEM demonstrated the uniform distribution and dispersion of the NPs throughout the PBAT matrix with slight agglomeration with MNP. PBAT nanocomposite films prepared by hot pressing not only showed an overall improvement in mechanical properties but also appreciable UV barrier properties, blocking nearly all the UV-A and over 90% UV-B light without severe sacrifice of optical transmittance. After 40 h of UV irradiation, PBAT−LMNP films exhibited a clear superiority over the other three systems, both in maintaining the UV shielding efficiency and the desirable mechanical performance. This study provides a promising solution to obtain novel cost-effective nanofillers with attractive functions and biodegradability, endowing the biodegradable PBAT films with enhanced mechanical, UV-barrier capacity and durability as well as biodegradability and, therefore, better potential in packaging or agricultural applications.

ASSOCIATED CONTENT

Supporting Information

The Supporting Information is available free of charge on the ACS Publications website at DOI: 10.1021/acssuschemeng.8b05755.

DLS curves for LNP prepared using ratios of filtrate and water at 1:2, 1:3, and 1:4; TGA scans and DSC curves of PBAT nanocomposites with 1.0 and 2.0 wt % NP loadings; and photographs and stress−strain curves for PBAT nanocomposite films; summary of tensile test results for neat PBAT and PBAT nanocomposite films before (0 h) and after the UV irradiation (40 h) (PDF)

DOI: 10.1021/acssuschemeng.8b05755
ACS Sustainable Chem. Eng. 2019, 7, 4147−4157

AUTHOR INFORMATION

Corresponding Authors

*E-mail: philippe.dubois@umons.ac.be (P. Dubois).
*E-mail: wenjunwang@zju.edu.cn (W.-J. Wang).
*E-mail: wulinbo@zju.edu.cn (L. Wu).

ORCID

Linbo Wu: 0000-0001-9964-6140
Wen-Jun Wang: 0000-0002-9740-2924

Notes

The authors declare no competing financial interest.

ACKNOWLEDGMENTS

Q.X., L.W., and W.-J.W. are grateful to the National Key Research and Development Program of China (2016YFB0302400) for financial support. P.D. thanks the Luxembourgish FNR for financial support in the frame of his PEARL chair.

REFERENCES

(1) Nowicki, M.; Richter, A.; Wolf, B.; Kaczmarek, H. Nanoscale mechanical properties of polymers irradiated by UV. *Polymer* **2003**, *44* (21), 6599−6606.
(2) Diepens, M.; Gijsman, P. Photodegradation of bisphenol A polycarbonate. *Polym. Degrad. Stab.* **2007**, *92* (3), 397−406.
(3) Coelho, C.; Hennous, M.; Verney, V.; Leroux, F. Functionalisation of polybutylene succinate nanocomposites: from structure to reinforcement of UV-absorbing and mechanical properties. *RSC Adv.* **2012**, *2* (12), 5430−5438.
(4) Calvo, M. E.; Castro Smirnov, J. R.; Míguez, H. Novel approaches to flexible visible transparent hybrid films for ultraviolet protection. *J. Polym. Sci., Part B: Polym. Phys.* **2012**, *50* (14), 945−956.
(5) Zayat, M.; Garcia-Parejo, P.; Levy, D. Preventing UV-light damage of light sensitive materials using a highly protective UV-absorbing coating. *Chem. Soc. Rev.* **2007**, *36* (8), 1270−1281.
(6) Yu, J. C.; Yu, J.; Ho, W.; Jiang, Z.; Zhang, L. Effects of F- Doping on the Photocatalytic Activity and Microstructures of Nanocrystalline TiO2 Powders. *Chem. Mater.* **2002**, *14* (9), 3808−3816.
(7) Maske, P. P.; Lokapure, S. G.; Nimbalkar, D.; Malavi, S.; D'Souza, J. I. In vitro determination of sun protection factor and chemical stability of Rosa kordesii extract gel. *J. Pharm. Res.* **2013**, *7* (6), 520−524.
(8) Jarzycka, A.; Lewińska, A.; Gancarz, R.; Wilk, K. A. Assessment of extracts of Helichrysum arenarium, Crataegus monogyna, Sambucus nigra in photoprotective UVA and UVB; photostability in cosmetic emulsions. *J. Photochem. Photobiol., B* **2013**, *128*, 50−57.
(9) Doherty, W. O. S.; Mousavioun, P.; Fellows, C. M. Value-adding to cellulosic ethanol: Lignin polymers. *Ind. Crops Prod.* **2011**, *33* (2), 259−276.
(10) Kaplan, D. L. Lignin. In *Biopolymers from renewable resources*; Springer: Berlin, 1998; Chapter 12, pp 292−322; DOI: 10.1007/978-3-662-03680-8_12.
(11) Glasser, W. G. Classification of lignin according to chemical and molecular structure. In *Lignin: Historical, Biological, and Materials Perspectives*; Northey, R. A., Glasser, W. G., Schultz, T. P., Eds.; ACS Symposium Series 742; American Chemical Society: Washington, DC, 2000; DOI: 10.1021/bk-2000-0742.ch009.
(12) Qian, Y.; Qiu, X.; Zhu, S. Lignin: a nature-inspired sun blocker for broad-spectrum sunscreens. *Green Chem.* **2015**, *17* (1), 320−324.
(13) Cruz, J. M.; Domínguez, J. M.; Domínguez, H.; Parajó, J. C. Antioxidant and Antimicrobial Effects of Extracts from Hydrolysates of Lignocellulosic Materials. *J. Agric. Food Chem.* **2001**, *49* (5), 2459−2464.
(14) Ugartondo, V.; Mitjans, M.; Vinardell, M. P. Comparative antioxidant and cytotoxic effects of lignins from different sources. *Bioresour. Technol.* **2008**, *99* (14), 6683−6687.
(15) Lindströmn, T. The colloidal behaviour of kraft lignin. *Colloid Polym. Sci.* **1979**, *257* (3), 277−285.
(16) Deng, Y.; Feng, X.; Yang, D.; Yi, C.; Qiu, X. Pi-Pi Stacking of the Aromatic Groups in Lignosulfonates. *BioResources* **2012**, *7* (1), 1145−1156.
(17) Wang, Y.; Xia, M.; Kong, X.; Severtson, S. J.; Wang, W.-J. Tailoring chain structures of L-lactide and ε-caprolactone copolyester macromonomers using rac-binaphthyl-diyl hydrogen phosphate-catalyzed ring-opening copolymerization with monomer addition strategy. *RSC Adv.* **2017**, *7* (46), 28661−28669.
(18) Frangville, C.; Rutkevičius, M.; Richter, A. P.; Velev, O. D.; Stoyanov, S. D.; Paunov, V. N. Fabrication of Environmentally Biodegradable Lignin Nanoparticles. *ChemPhysChem* **2012**, *13* (18), 4235−4243.
(19) Yearla, S. R.; Padmasree, K. Preparation and characterisation of lignin nanoparticles: evaluation of their potential as antioxidants and UV protectants. *J. Exp. Nanosci.* **2016**, *11* (4), 289−302.
(20) Gilca, I. A.; Popa, V. I.; Crestini, C. Obtaining lignin nanoparticles by sonication. *Ultrason. Sonochem.* **2015**, *23*, 369−375.
(21) Gilca, I. A.; Ghitescu, R. E.; Puitel, A. C.; Popa, V. I. Preparation of lignin nanoparticles by chemical modification. *Iran. Polym. J.* **2014**, *23* (5), 355−363.
(22) Ge, Y.; Wei, Q.; Li, Z. Preparation and Evaluation of the Free Radical Scavenging Activities of Nanoscale Lignin Biomaterials. *BioResources* **2014**, *9* (4), 6699−6706.
(23) Nair, S. S.; Sharma, S.; Pu, Y.; Sun, Q.; Pan, S.; Zhu, J. Y.; Deng, Y.; Ragauskas, A. J. High Shear Homogenization of Lignin to Nanolignin and Thermal Stability of Nanolignin-Polyvinyl Alcohol Blends. *ChemSusChem* **2014**, *7* (12), 3513−3520.
(24) Del Saz-Orozco, B.; Oliet, M.; Alonso, M. V.; Rojo, E.; Rodríguez, F. Formulation optimization of unreinforced and lignin nanoparticle-reinforced phenolic foams using an analysis of variance approach. *Compos. Sci. Technol.* **2012**, *72* (6), 667−674.
(25) Yang, W.; Dominici, F.; Fortunati, E.; Kenny, J.; Puglia, D. Effect of lignin nanoparticles and masterbatch procedures on the final properties of glycidyl methacrylate-g-poly (lactic acid) films before and after accelerated UV weathering. *Ind. Crops Prod.* **2015**, *77*, 833−844.
(26) Guo, G.; Zhang, C.; Du, Z.; Zou, W.; Tian, H.; Xiang, A.; Li, H. Structure and property of biodegradable soy protein isolate/PBAT blends. *Ind. Crops Prod.* **2015**, *74*, 731−736.
(27) Chaochanchaikul, K.; Jayaraman, K.; Rosarpitak, V.; Sombatsompop, N. Influence of lignin content on photodegradation in wood/HDPE composites under UV weathering. *BioResources* **2011**, *7* (1), 0038−0055.
(28) Prota, G. Natrual and synthetic melanins. In *Melanins and Melagenesis*; Academic Press, Inc.: San Diego, 1992.
(29) Brenner, M.; Hearing, V. J. The Protective Role of Melanin Against UV Damage in Human Skin†. *Photochem. Photobiol.* **2008**, *84* (3), 539−549.
(30) Wang, Y.; Li, T.; Ma, P.; Bai, H.; Xie, Y.; Chen, M.; Dong, W. Simultaneous Enhancements of UV-Shielding Properties and Photostability of Poly(vinyl alcohol) via Incorporation of Sepia Eumelanin. *ACS Sustainable Chem. Eng.* **2016**, *4* (4), 2252−2258.
(31) Wang, Y.; Li, T.; Wang, X.; Ma, P.; Bai, H.; Dong, W.; Xie, Y.; Chen, M. Superior Performance of Polyurethane Based on Natural Melanin Nanoparticles. *Biomacromolecules* **2016**, *17* (11), 3782−3789.
(32) Shanmuganathan, K.; Cho, J. H.; Iyer, P.; Baranowitz, S.; Ellison, C. J. Thermooxidative Stabilization of Polymers Using Natural and Synthetic Melanins. *Macromolecules* **2011**, *44* (24), 9499−9507.
(33) Lee, H.; Dellatore, S. M.; Miller, W. M.; Messersmith, P. B. Mussel-Inspired Surface Chemistry for Multifunctional Coatings. *Science* **2007**, *318* (5849), 426−430.
(34) Wang, W.; Jiang, Y.; Wen, S.; Liu, L.; Zhang, L. Preparation and characterization of polystyrene/Ag core−shell microspheres − A bio-inspired poly(dopamine) approach. *J. Colloid Interface Sci.* **2012**, *368* (1), 241−249.

DOI: 10.1021/acssuschemeng.8b05755
ACS Sustainable Chem. Eng. 2019, 7, 4147−4157

(35) Lu, Y.; Zhu, H.; Wang, W.-J.; Li, B.-G.; Zhu, S. Collectable and Recyclable Mussel-Inspired Poly(ionic liquid)-Based Sorbents for Ultrafast Water Treatment. *ACS Sustainable Chem. Eng.* **2017**, *5* (4), 2829−2835.
(36) Muthuraj, R.; Misra, M.; Mohanty, A. Hydrolytic degradation of biodegradable polyesters under simulated environmental conditions. *J. Appl. Polym. Sci.* **2015**, *132* (27), 42189.
(37) Södergård, A.; Stolt, M. Properties of lactic acid based polymers and their correlation with composition. *Prog. Polym. Sci.* **2002**, *27* (6), 1123−1163.
(38) Van de Velde, K.; Kiekens, P. Biopolymers: overview of several properties and consequences on their applications. *Polym. Test.* **2002**, *21* (4), 433−442.
(39) Kijchavengkul, T.; Auras, R.; Rubino, M.; Selke, S.; Ngouajio, M.; Fernandez, R. T. Biodegradation and hydrolysis rate of aliphatic aromatic polyester. *Polym. Degrad. Stab.* **2010**, *95* (12), 2641−2647.
(40) Li, J.; Lai, L.; Wu, L.; Severtson, S. J.; Wang, W.-J. Enhancement of Water Vapor Barrier Properties of Biodegradable Poly(butylene adipate-co-terephthalate) Films with Highly Oriented Organomontmorillonite. *ACS Sustainable Chem. Eng.* **2018**, *6* (5), 6654−6662.
(41) Xing, Q.; Ruch, D.; Dubois, P.; Wu, L.; Wang, W.-J. Biodegradable and High-Performance Poly(butylene adipate-co-terephthalate)−Lignin UV-Blocking Films. *ACS Sustainable Chem. Eng.* **2017**, *5* (11), 10342−10351.
(42) Abächerli, A.; Doppenberg, F., Method for preparing alkaline solutions containing aromatic polymers. U.S. Patent US6239198B1, 2001.
(43) Constant, S.; Wienk, H. L.; Frissen, A. E.; de Peinder, P.; Boelens, R.; Van Es, D. S.; Grisel, R. J.; Weckhuysen, B. M.; Huijgen, W. J.; Gosselink, R. J.; Bruijnincx, P. C. A. New insights into the structure and composition of technical lignins: a comparative characterisation study. *Green Chem.* **2016**, *18* (9), 2651−2665.
(44) Buono, P.; Duval, A.; Verge, P.; Averous, L.; Habibi, Y. New insights on the chemical modification of lignin: acetylation versus silylation. *ACS Sustainable Chem. Eng.* **2016**, *4* (10), 5212−5222.
(45) Ju, K.-Y.; Lee, Y.; Lee, S.; Park, S. B.; Lee, J.-K. Bioinspired Polymerization of Dopamine to Generate Melanin-Like Nanoparticles Having an Excellent Free-Radical-Scavenging Property. *Biomacromolecules* **2011**, *12* (3), 625−632.
(46) Schubert, S.; Delaney, J. T., Jr.; Schubert, U. S. Nanoprecipitation and nanoformulation of polymers: from history to powerful possibilities beyond poly(lactic acid). *Soft Matter* **2011**, *7* (5), 1581−1588.
(47) Yildiz, M. E.; Prud'homme, R. K.; Robb, I.; Adamson, D. H. Formation and characterization of polymersomes made by a solvent injection method. *Polym. Adv. Technol.* **2007**, *18* (6), 427−432.
(48) Meng, F.; Hiemstra, C.; Engbers, G. H. M.; Feijen, J. Biodegradable Polymersomes. *Macromolecules* **2003**, *36* (9), 3004−3006.
(49) Herlinger, E.; Jameson, R. F.; Linert, W. Spontaneous autoxidation of dopamine. *J. Chem. Soc., Perkin Trans. 2* **1995**, No. 2, 259−263.
(50) Lee, H.; Rho, J.; Messersmith, P. B. Facile Conjugation of Biomolecules onto Surfaces via Mussel Adhesive Protein Inspired Coatings. *Adv. Mater.* **2009**, *21* (4), 431−434.
(51) Ye, Q.; Zhou, F.; Liu, W. Bioinspired catecholic chemistry for surface modification. *Chem. Soc. Rev.* **2011**, *40* (7), 4244−4258.
(52) Yang, D.; Tian, M.; Wang, W.; Li, D.; Li, R.; Liu, H.; Zhang, L. Controllable dielectric and electrical performance of polymer composites with novel core/shell-structured conductive particles through biomimetic method. *Electrochim. Acta* **2013**, *87*, 9−17.
(53) She, D.; Xu, F.; Geng, Z.; Sun, R.; Jones, G. L.; Baird, M. S. Physicochemical characterization of extracted lignin from sweet sorghum stem. *Ind. Crops Prod.* **2010**, *32* (1), 21−28.
(54) Zangmeister, R. A.; Morris, T. A.; Tarlov, M. J. Characterization of Polydopamine Thin Films Deposited at Short Times by Autoxidation of Dopamine. *Langmuir* **2013**, *29* (27), 8619−8628.
(55) Simonovic, B.; Vucelic, V.; Hadzi-Pavlovic, A.; Stepien, K.; Wilczok, T.; Vucelic, D. Thermogravimetry and differential scanning calorimetry of natural and synthetic melanins. *J. Therm. Anal.* **1990**, *36* (7−8), 2475−2482.
(56) Dizhbite, T.; Telysheva, G.; Jurkjane, V.; Viesturs, U. Characterization of the radical scavenging activity of lignins−natural antioxidants. *Bioresour. Technol.* **2004**, *95* (3), 309−317.
(57) Chivrac, F.; Pollet, E.; Avérous, L. Nonisothermal crystallization behavior of poly(butylene adipate-co-terephthalate)/clay nano-biocomposites. *J. Polym. Sci., Part B: Polym. Phys.* **2007**, *45* (13), 1503−1510.
(58) Kashani Rahimi, S.; Aeinehvand, R.; Kim, K.; Otaigbe, J. U. Structure and Biocompatibility of Bioabsorbable Nanocomposites of Aliphatic-Aromatic Copolyester and Cellulose Nanocrystals. *Biomacromolecules* **2017**, *18* (7), 2179−2194.
(59) Wang, Y.; Weng, F.; Li, J.; Yu, W.; Severtson, S. J.; Wang, W.-J.; Lai, L. Influence of Phase Separation on Performance of Graft Acrylic Pressure Sensitive Adhesives with Various Copolyester Side Chains. *ACS Omega* **2018**, *3* (6), 6945−6954.
(60) Masson, F.; Decker, C.; Andre, S.; Andrieu, X. UV-curable formulations for UV-transparent optical fiber coatings: I. Acrylic resins. *Prog. Org. Coat.* **2004**, *49* (1), 1−12.
(61) Sadeghifar, H.; Venditti, R.; Jur, J.; Gorga, R. E.; Pawlak, J. J. Cellulose-Lignin Biodegradable and Flexible UV Protection Film. *ACS Sustainable Chem. Eng.* **2017**, *5* (1), 625−631.
(62) Chung, Y.-L.; Olsson, J. V.; Li, R. J.; Frank, C. W.; Waymouth, R. M.; Billington, S. L.; Sattely, E. S. A renewable lignin−lactide copolymer and application in biobased composites. *ACS Sustainable Chem. Eng.* **2013**, *1* (10), 1231−1238.
(63) Jiang, Y.; Song, Y.; Miao, M.; Cao, S.; Feng, X.; Fang, J.; Shi, L. Transparent nanocellulose hybrid films functionalized with ZnO nanostructures for UV-blocking. *J. Mater. Chem. C* **2015**, *3* (26), 6717−6724.
(64) Feng, X.; Zhao, Y.; Jiang, Y.; Miao, M.; Cao, S.; Fang, J. Use of carbon dots to enhance UV-blocking of transparent nanocellulose films. *Carbohydr. Polym.* **2017**, *161*, 253−260.
(65) Kijchavengkul, T.; Auras, R.; Rubino, M.; Ngouajio, M.; Fernandez, R. T. Assessment of aliphatic−aromatic copolyester biodegradable mulch films. Part I: Field study. *Chemosphere* **2008**, *71* (5), 942−953.
(66) Toh, K.; Nakano, S.; Yokoyama, H.; Ebe, K.; Gotoh, K.; Noda, H. Anti-deterioration Effect of Lignin as an Ultraviolet Absorbent in Polypropylene and Polyethylene. *Polym. J.* **2005**, *37* (8), 633−635.
(67) Majer, Z.; Hutař, P.; Náhlík, L. Determination of the Effect of Interphase on the Fracture Toughness and Stiffness of a Particulate Polymer Composite. *Mech. Compos. Mater.* **2013**, *49* (5), 475−482.
(68) Gu, C.; Hauge, D. A.; Severtson, S. J.; Wang, W.-J.; Gwin, L. E. Effect of Poly(l-lactide-co-ε-caprolactone) Macromonomer Composition on the Properties of Hot-Melt Adhesives with High Biomass Contents. *Ind. Eng. Chem. Res.* **2014**, *53* (44), 17376−17385.
(69) Sun, Y.; Yang, L.; Lu, X.; He, C. Biodegradable and renewable poly(lactide)-lignin composites: synthesis, interface and toughening mechanism. *J. Mater. Chem. A* **2015**, *3* (7), 3699−3709.
(70) Yang, W.; Fortunati, E.; Dominici, F.; Giovanale, G.; Mazzaglia, A.; Balestra, G. M.; Kenny, J. M.; Puglia, D. Synergic effect of cellulose and lignin nanostructures in PLA based systems for food antibacterial packaging. *Eur. Polym. J.* **2016**, *79*, 1−12.
(71) Weng, F.; Li, X.; Wang, Y.; Wang, W. J.; Severtson, S. J. Kinetics and Modeling of Ring Opening Copolymerization of L-lactide and ε-Caprolactone. *Macromol. React. Eng.* **2015**, *9* (6), 535−544.

DOI: 10.1021/acssuschemeng.8b05755
ACS Sustainable Chem. Eng. 2019, 7, 4147−4157